npj | Flexible Electronics

www.nature.com/npjflexelectron

ARTICLE OPEN

Highly sensitive integrated flexible tactile sensors with piezoresistive $Ge_2Sb_2Te_5$ thin films

Zhiguang Wang[1,2,3], Cunzheng Dong[1], Xinjun Wang[1], Menghui Li[1], Tianxiang Nan[1], Xianfeng Liang[1], Huaihao Chen[1], Yuyi Wei[1], Haomiao Zhou[1,4], Mohsen Zaeimbashi[1], Syd Cash[3] and Nian-Xiang Sun[1]

Flexible tactile sensor has been extensively investigated as a key component for emerging electronics applications such as robotics, wearable devices, computer hardware, and security systems. Tactile sensors based on various one-dimensional materials have been widely explored. However, precise control of the direction and distribution of these nanomaterials remains a great challenge, and it has been difficult to scale down the device. Here, we introduce highly sensitive integrated flexible tactile sensors based on uniform phase-change $Ge_2Sb_2Te_5$ (GST) thin films that can scale device size down, at least, to micrometer range. Significant piezoresistive effect has been observed in GST-based sensors, showing a giant gauge factor of 338. A proof of concept 5 × 5 sensor array functioning as a touch panel has been demonstrated. Also, the flexible GST tactile sensor has been utilized for monitoring of radial artery pulse. In addition to the well-known tunable electrical and optical properties, the piezoresistive GST films provide a versatile platform for the integration of sensing, recording, and displaying functions.

npj Flexible Electronics (2018)2:17 ; doi:10.1038/s41528-018-0030-4

INTRODUCTION

Flexible tactile sensors are of paramount importance for the development of various future applications, including flexible touch display,[1] electronic skin,[2–4] health monitoring devices,[5,6] and energy harvesting devices.[7–9] Compared with tactile sensors based on other physical effects (e.g. piezoelectric, capacitive, optical, magnetic, ultrasonic and triboelectronic[10–13]), piezoresistive tactile sensors have the advantages of high sensitivity, planar device design, excellent flexibility, and simple read-out electronics.[14–20]

Various nanomaterials including organic/inorganic matrix arrays, hybrid composites, and nanowire or nanotube assemblies have been integrated on flexible substrates for development of flexible tactile sensors.[9,21] Despite the potential and high performance of these devices, it is still a great challenge to fabricate a wearable, multiplex tactile sensor array due to their complicated fabrication process and delicate conduction mechanism (percolation, quantum tunneling, etc.). More importantly, one intrinsic problem with these nanomaterials is the lack of uniformity that makes it difficult to fabricate highly integrated devices on an industrial scale. Most of the sensors based on these nanomaterials can only give a spatial resolution in millimeter range whereas certain applications such as touch screen and fingerprint recognition require spatial resolution down to micrometer range.[2,22–25]

In addition, tactile sensors have been designed with widely adopted semiconductors, e.g. Si or Ge. The major drawbacks of these sensors are their fragility and rigidity. High temperature oxidizing and doping procedures are necessary during the fabrication which make it impossible to develop Si/Ge-based sensors on flexible substrates whose melting points are usually below 300 °C.[26] These disadvantages can be partly overcome by embedding the rigid sensors in flexible polymers.[27–29] However, this complicated process inevitably sacrifices the sensitivity and the miniaturization of the semiconductor sensors, resulting in bulky piezoresistive sensor with loose performance. An optimal material, therefore, for the design of flexible tactile sensor with high spatial resolution should be highly piezoresistive, uniform, and easy to produce at room temperature.

GST has been widely studied as information recording medium due to a giant optical and electronic property change around the crystallization temperature. Tunable electrical resistance change has been reported by Ma et al. in 2012.[30] However, a huge pressure up to 28 GPa has to be used to induce the amorphous to body-center-cubic crystal phase transformation. The electrical response in GST thin films under subtle mechanical pressure, to the best of our knowledge, has not been investigated.

Here, we report on new integrated flexible tactile sensors based on uniform and homogeneous piezoresistive GST thin films coated on flexible substrates. A high GF value of 338 has been observed in our flexible GST strain sensor with a limit of detection ~50 parts per billion (ppb). More importantly, GST sensors with a feature size of 1 μm has been fabricated and characterized, promising a spatial resolution of >12,700 pixels per inch (PPI). A proof of concept 5 × 5 touching sensor array has been prepared to show the promising application of touching screen.

RESULTS AND DISCUSSIONS

GST has received tremendous amount of research interest due to the fact that it can alternate between crystalline and amorphous phases more quickly than any other material yet studied.[31] These

[1]Department of Electrical and Computer Engineering, Northeastern University, Boston, MA 02115, USA; [2]Electronic Materials Research Laboratory, Key Laboratory of the Ministry of Education & International Center for Dielectric Research, School of Electronic and Information Engineering, Xi'an Jiaotong University, 710049 Xi'an, China; [3]Department of Neurology, Massachusetts General Hospital, Boston, MA 02114, USA and [4]College of Information Engineering, China Jiliang University, 310018 Hangzhou, China
Correspondence: Zhiguang Wang (zgwang18@xjtu.edu.cn) or Syd Cash (scash@mgh.harvard.edu) or Nian-Xiang Sun (n.sun@neu.edu)

Received: 26 January 2018 Revised: 12 April 2018 Accepted: 20 April 2018
Published online: 15 June 2018

phase changes result from changes in the bonds between atoms, which also modify the electronic and optical properties of GST.[32] GST has been studied as one of the most promising candidates for next generation of universal memory due to its extraordinary properties such as extreme scalability, fast switching speeds, and high switching endurance. Also, electrically induced stable color changes in both reflective and semi-transparent modes in GST have been reported, indicating possible applications in display and data visualization devices.[33–35] More recently, amorphous to crystalline phase transition in GST has been realized by applying a pressure of 28 GPa, demonstrating a dramatic change of up to four orders in electrical resistance due to piezoresistive effect.[30]

To assess the ability of our GST film to function as a strain sensor, we deposited 100 nm GST thin films on flexible polyethylene terephthalate (PET) foils with a thickness of 100 μm and fabricated a cantilever structure that is one of the most ubiquitous structures in the field of microelectromechanical systems for sensing applications.[36–40] Patterned Ti electrodes were prepared through photo lithography process on top of GST film, as shown in Fig. 1a. The piezoresistor loop is formed by two legs with width of 1 mm. The horizontal strain ε distributed along the top surface of the cantilever is proportional to the value of $l-x$, where l is the length of the cantilever and x is the distance from the base. Therefore, the exposed GST stripe is placed at the root of the cantilever to guarantee a maximum strain due to bending. Figure 1b shows the resistance variation ($\Delta R/R$) with different bending conditions. A resistance change up to 50% can be easily obtained by bending the tip of the cantilever (length 2 cm) down for 3 mm. By bending the cantilever up and down with a tweezer, we can apply compressive and tensile strain in the GST film, respectively. With a compressive strain, the change in atomic arrangements and bonding can reduce the low-electron-density regions, which contributes to the narrowing of band gap and delocalization of trapped electrons, as revealed by ab initio molecular dynamics simulation.[30,33,41] In consequence, the resistance in GST film will decrease when bent up and increase when bent down. With further bending of the cantilever a resistance change up to 150% can be obtained, as shown in Supplementary Movie 1 (from 23 MΩ to 58 MΩ).

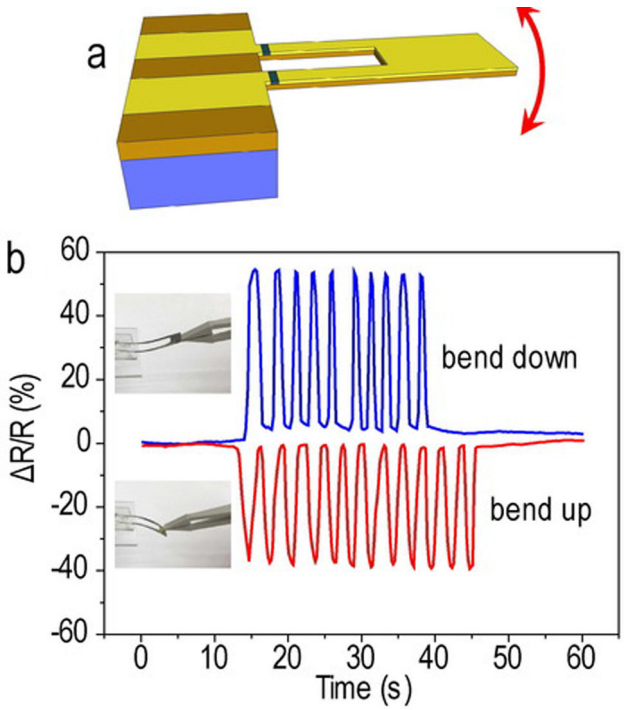

Fig. 1 GST cantilever strain sensor. **a** Schematic illustration of the GST-based strain sensor with GST strip at the root of the cantilever. **b** Time-resolved electrical response of the GST sensor with different bending conditions

To quantitatively determine the gauge factor of the GST-based strain sensor, we then adopted piezoelectric PZT for the generation of strain through electromechanical coupling. Flexible strain sensor was prepared by patterning top electrodes with a gap of 20 μm on top of 100 nm GST layer grown on PET. The sensor was then attached on 3-mm-thick $Pb[Zr_{0.52}Ti_{0.48}]O_3$ (PZT) ($d_{33} = 500$ pm/V) slab with West System epoxy, as shown in Fig. 2b. Then the electromechanical strain from the PZT slab can be calculated by $\varepsilon = d_{33}{\cdot}E$, where E is the electric field on the PZT component. With a periodic $E = A{\cdot}\sin(t)$, a periodic strain can be generated which then induces a periodic resistance change in GST component.

Figure 2c shows the fast Fourier transform (FFT) spectrum analysis of the electrical response in flexible strain sensor with and without strain signal. The $1/f$ noise behavior is obvious, showing a decreasing noise power spectral density with increasing frequency. One strong peak at 1 Hz can be observed as a consequence of the 1 Hz strain from the piezoelectric PZT. The signal to noise ratio (SNR) is calculated by $SNR = 20\log_{10}(A_{signal}/A_{noise})$, where A_{signal} is the amplitude of the power spectral density of electrical response from the strain sensor due to strain and A_{noise} is the amplitude of the power spectral density of noise. LOD = 50 ppb can be determined by the linear fit of the SNR-ε curve, as shown in Fig. 2d. This value is comparable with the best commercialized strain sensor based on rigid Si or Ge.

The gauge factor is one of the most important parameters for evaluation of the strain gauge. And it can be expressed as $GF = (\Delta R/R)/\varepsilon$, where ε is the strain, ΔR is the resistance change, and R is unstrained resistance of the gauge. Figure 3 shows the plot of relative resistance change as a function of applied strain, where a linear fit indicating GF = 338 can be clearly deduced. One should note that this value is much larger than that of recently reported various nanostructured piezoresistive materials: graphene-based film[42](GF = 6.1), interlocking nanofibers[21] (GF = 11.45), gold nanowires[19] (GF = 7.38). More importantly, the GF of our GST-based strain sensor is more than two times larger than that of commercially available Si- or Ge-based strain gauges. Detailed results about resistance change as a function of external strain can be found in Supplementary Fig. 1. The combination of high GF and excellent flexibility makes the GST-based strain sensor a strong competitor to traditional semiconductor strain gauge and one of the best candidates for next-generation flexible and wearable strain sensors for health monitoring and e-skin.

Next, we measured the frequency response of the GST-based strain sensor, as shown in Fig. 4. Obvious periodic peaks of relative resistance change are determinable for the 3000 ppb strain signal with frequencies from 1 to 100 Hz, as shown in Supplementary Fig. 2. The root mean square values of the relative resistance ($RMS_{\Delta R/R}$) at different frequency are shown in Fig. 4d. No obvious degradation in the electrical response has been observed as the measurement frequency increased from 1 to 100 Hz, indicating a small delay time in GST strain sensor with external stimuli, as shown in Supplementary Movie 2.

Figure 5 demonstrates the proof of concept test of GST-based 5×5 sensor array as a touch sensing panel. Each sensor unit comprises of patterned Cu electrodes separated by 0.3×3.5 mm GST stripe. By pressing the GST area, the resistance between patterned Cu electrodes can be changed accordingly. The electrical signal from the strain sensor array was then fed into a preamplifier with band pass frequency between 0.18 and 18 Hz and a gain of 200×. The output signal was connected directly to the USB-compatible DAQ device and the data were then transmitted to PC through serial port. LabVIEW software has been

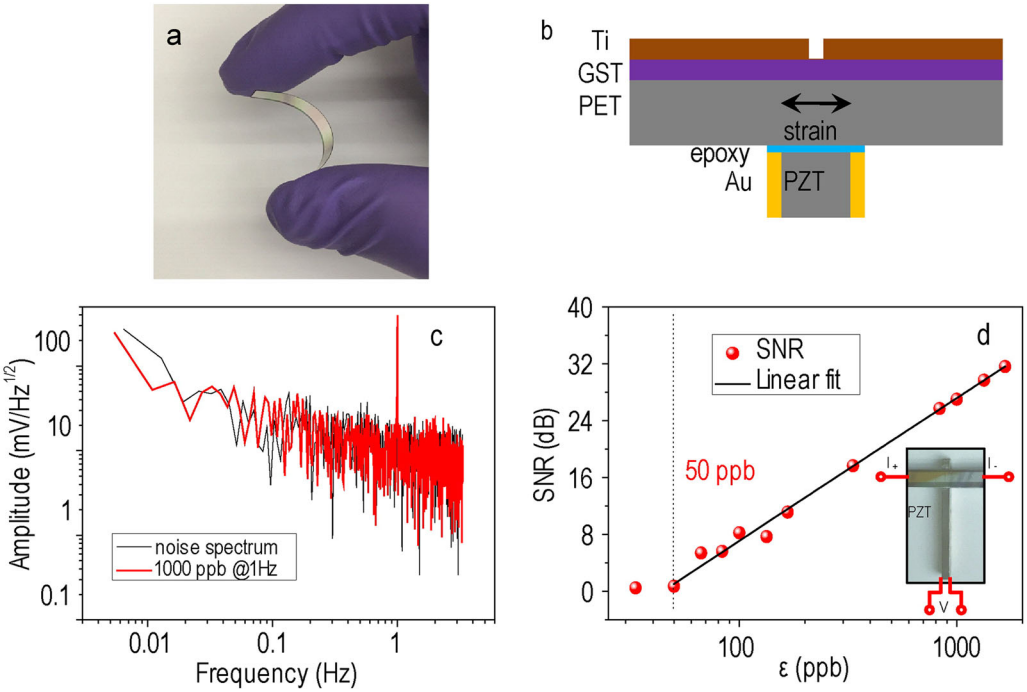

Fig. 2 **a** Photograph showing the flexibility of the GST strain sensor. **b** Schematic illustration of the GST sensor attached to a piezoelectric PZT slab. **c** Spectrum analysis of the electrical response in GST strain sensor with and without strain. **d** SNR curve of the sensor showing a limit of detection of 50 ppb

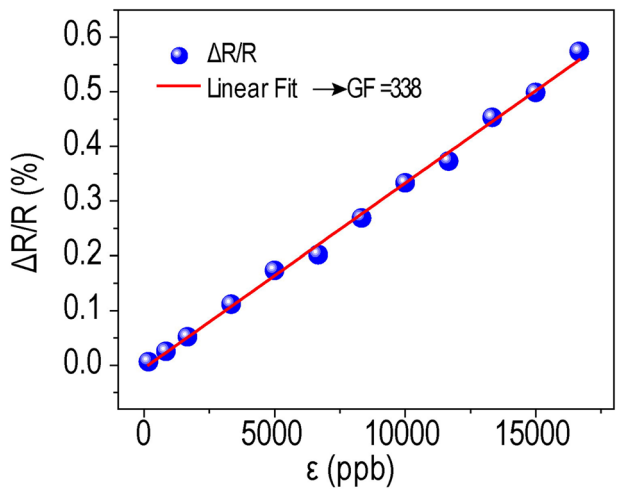

Fig. 3 Normalized resistance change as a function of external strain, demonstrating a GF of 338

used to analyze and display the results in a three-dimensional figure, as shown in Fig. 5b and Supplementary Movie 3. Addressable electrical outputs around 2 V have been recorded, indicating a resistance change around 5% in the touching sensor units. In addition, electrically induced stable color changes in both reflective and semi-transparent modes of a few nanometer thick GST film has been reported,[32] indicating that GST thin film can function as both displaying and sensing elements simultaneously. These finds have clearly demonstrated the possibility of using our GST strain sensors as tactile sensing and touching display devices.

Next, we fabricated small-sized GST strain sensors to demonstrate the most important advantage of the proposed GST sensor compared with other one-dimensional nanomaterials: the unique scaling advantage of having better performance with smaller sizes. GST thin films with thickness 2–3 nm have shown more than three orders of resistance change due to phase transition.[31] The limit to which GST thin film can be scaled is hence limited by lithography at least until 45 nm. Thus, it offers the biggest potential of achieving strain sensor with ultra-high spatial resolution and memory with ultra-high recording density.

Figure 6a shows the schematic illustration of the cross-sectional image of sensor with small feature size down to 1 μm. Cu patterns with a thickness of 100 nm and 1 μm in-plane gaps with each other were prepared on PET foil by magnetron sputtering and optical lithography technique. And then, patterned GST was prepared on the specific areas by lift-off process for sensing of touching induced strain.

Figure 6b shows the microscope image of 4 μm size GST strain sensor. The GST stripe between Cu electrodes has a dimension of 1 × 12 μm. An oscilloscope has been used to measure the current change through a constant reference resistor in serial connection with the strain sensor. Figure 6c shows the normalized resistance change as a function of the touching behavior (inset photograph). An obvious change of up to 5% in resistance has been observed, promising a spatial resolution of up to 12,700 PPI, which is more than 23 times larger than the widely adopted 550 PPI spatial resolution in touch screen technology and iPhone's TouchID. One should note that the above-mentioned spatial resolution is confined by the lithography technique available to us but not limited by the intrinsic scalability of the GST materials. Much higher spatial resolution can be achieved with improved processing technique for certain applications such as high resolution fingerprint recognition.[1,43]

Finally, the flexible GST strain sensor was used to monitor the pulse of human radial artery in real time. The resistance of the sensor was measured before and after physical exercise, as shown in Fig. 7a, b, respectively. Figure 7c shows the FFT analysis of the obtained results where an obvious increased pulse rate from 1.17 to 1.41 Hz after physical exercise has been demonstrated. Figure 7d shows the closer view of the pulse waveform, where both the

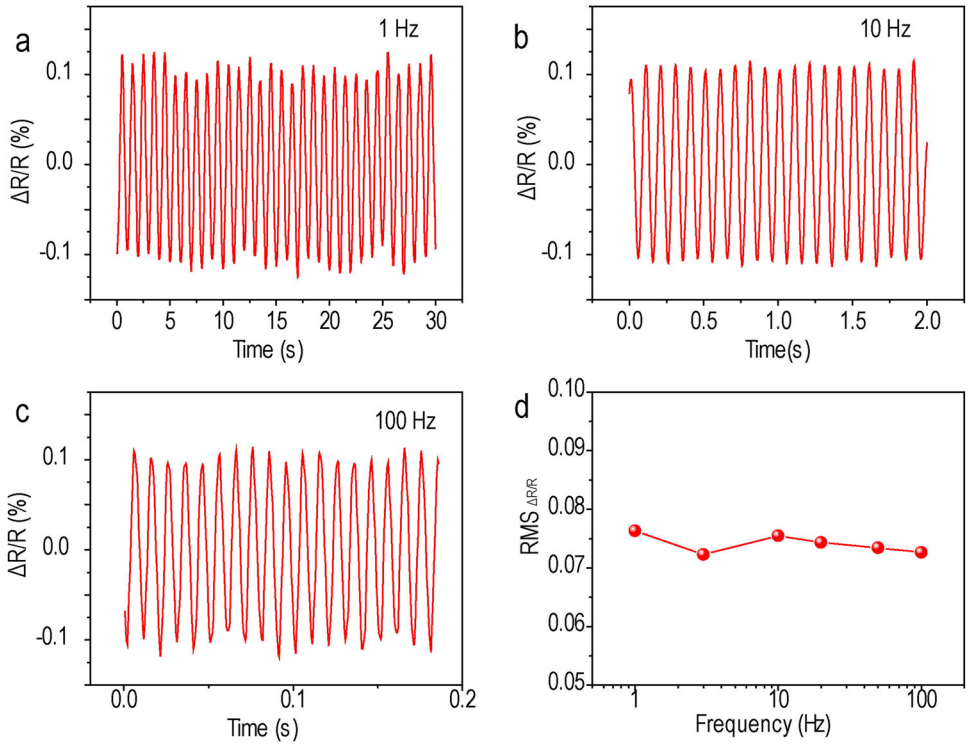

Fig. 4 Time-resolved electrical response of the GST sensor with strain signal changing from 1 to 100 Hz

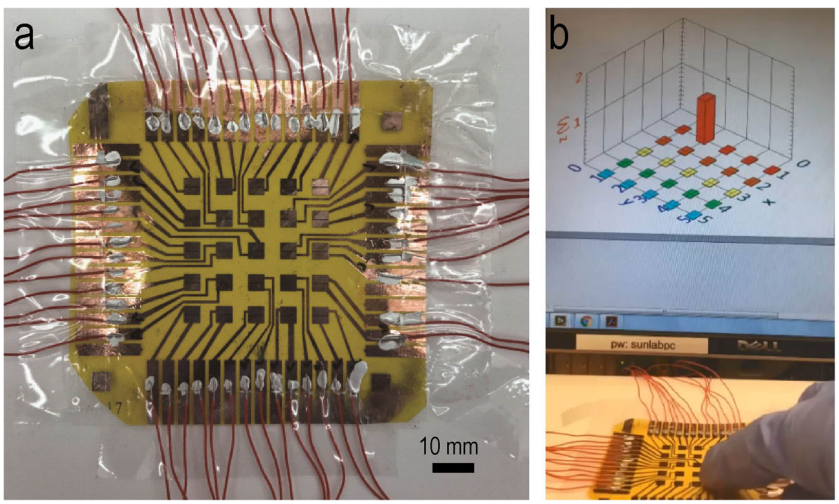

Fig. 5 **a** Photograph of the GST-based 5 × 5 sensor array on flexible PET foil (scale bar, 10 mm). **b** 3D illustration of the electrical response of sensor with touching behavior

forward moving wave and the reflected wave can be recognized. These results can be used for the determination of arterial stiffness and blood pressure,[7,44] indicating that the flexible strain sensor based on GST films can be used as wearable diagnostic device for human health monitoring.

CONCLUSION

In summary, we have demonstrated highly sensitive novel integrated flexible tactile sensors based on the remarkable piezoresistive effect in homogeneous GST thin films, which can be also used as excellent strain sensors for various applications. Room temperature growth of GST thin film provides more freedom for selection of various flexible substrates. A large GF of 338 has been achieved from flexible GST strain sensor which is two times larger than its rigid counterpart based on Si or Ge. A proof of concept 5 × 5 flexible sensor array has been demonstrated. More importantly, GST strain sensor with feature size of 1 μm (the size is only limited by the processing technique but not the intrinsic scalability of the GST material) has been fabricated and characterized, promising a spatial resolution of 12,700 PPI. Also, the GST flexible sensor can function as wearable device for monitoring of radial artery pulse. The giant piezoresistive effect, excellent flexibility, and nanometer scalability in GST thin films make it suitable for applications in consumer and mobile electronic devices.

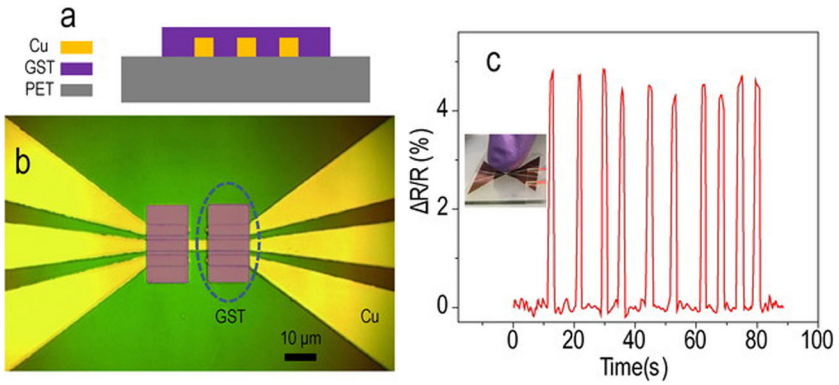

Fig. 6 **a** Cross-sectional schematic of the GST sensor. **b** Optical microscopy image of the flexible strain sensor with 1 μm GST gap (scale bar, 10 μm). **c** Relative resistance change with touching behavior

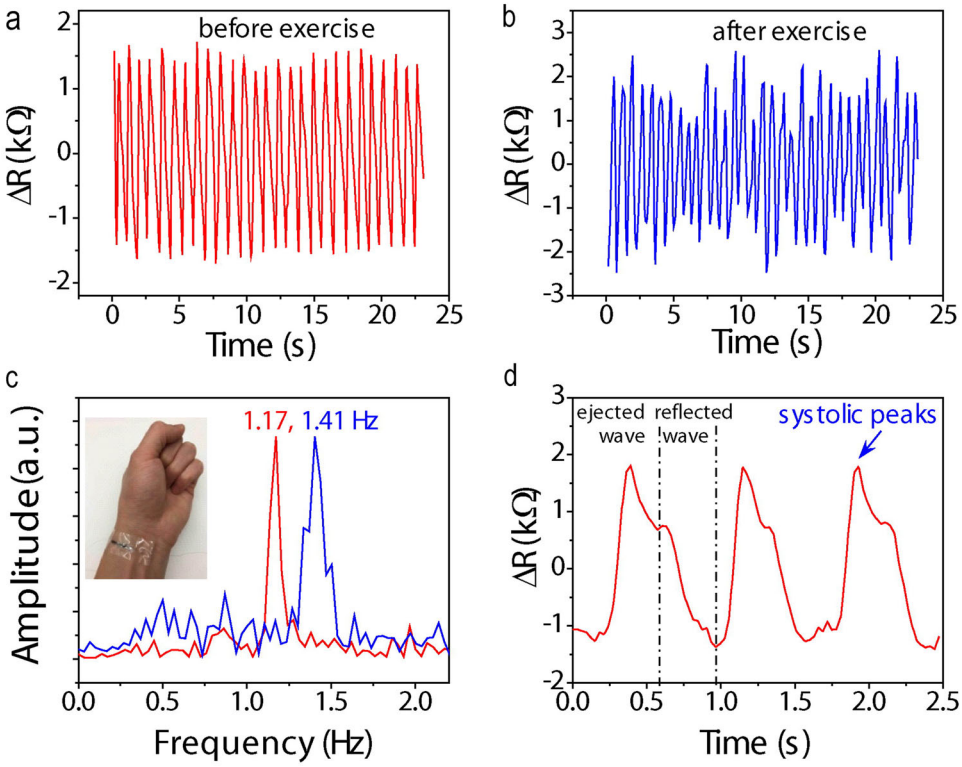

Fig. 7 **a, b** Real-time resistance change in the GST sensor that was attached to radial artery before and after physical exercise, respectively. **c** FFT analysis of the resistance change. **d** Closer view of the resistance change due to pulse wave, showing obvious ejected and reflected waves

METHODS

Device fabrication

Commercial PET flexible foil with thickness of 100 μm was used as substrate. GST layer with a thickness of 100 nm was deposited at room temperature by dc magnetron sputtering. The base pressure of the sputtering system was 10^{-8} Torr. Argon with a purity of 99.998% was introduced as a working gas. And the sputtering pressure was kept at 3 mTorr. Patterned Ti and Cu electrodes with a thickness of 100 nm were prepared with optical lithography and lift-off techniques. Negative photoresist (AZ nLOF 2020) was spun onto the substrates (4000 rotations per min for 40 s), forming a uniform photoresist sacrifice layer with a thickness of ~1.8 μm. Softbake was carried out on hotplate at 115 °C for 60 s, followed by exposure at 365 nm, 275 W for 10 s with designed Cr mask. And then, post-exposure bake was carried at 115 °C for 60 s. The developing process was carried at room temperature for 120 s within AZ 300 MIF developer. Micro Automation-Model 1006 Dicing Saw was used for the cutting of the Ti/GST/PET heterostructures to form a split leg cantilever. The cantilever was fixed on glass with glue.

Electrical measurements

For the gauge factor test, the backside of the GST sensor with a total thickness of 100 μm was attached to a piezoelectric PZT slab with mixed WEST System 105 and 206 epoxy resin. SR 830 lock-in amplifier connected with Carvin DCM1000 power amplifier was used to drive the PZT slab with frequency from 1 to 100 Hz. The resistance in the GST sensor was measured by Keithley Series 2700 multimeter. The GST sensor array was connected with 100 kΩ resistors and the voltage variation on each resistor was fed into a customer-made band pass filter and preamplifier. The data were recorded by Arduino Mega 2560 and visualized through LabVIEW software.

Data availability

The datasets generated and analyzed during the current study are available from the corresponding authors on reasonable request.

ACKNOWLEDGEMENTS

The work was financially supported by W.M. Keck Foundation. We thank Scott McNamara and Sivasubramanian Somu for useful discussion about microfabrication. And we thank Kostas Nanoscale Research Center at Northeastern University and Center for Nanoscale Systems at Harvard University for fabrication and characterization facilities.

AUTHOR CONTRIBUTIONS

Z.W. conceived the idea of this research, Z.W. and C.D. carried out the experiments. Z. W., X.W., and M.L. performed data analysis. N.-X.S. and S.C. supervised and coordinated the study. All authors discussed the results and jointly wrote the manuscript.

ADDITIONAL INFORMATION

Supplementary information accompanies the paper on the *npj Flexible Electronics* website (https://doi.org/10.1038/s41528-018-0030-4).

Competing interests: The authors declare no competing interests.

Publisher's note: Springer Nature remains neutral with regard to jurisdictional claims in published maps and institutional affiliations.

REFERENCES

1. Wang, J. et al. Rod-coating: towards large-area fabrication of uniform reduced graphene oxide films for flexible touch screens. *Adv. Mater.* **24**, 2874–2878 (2012).
2. Zhu, G. et al. Self-powered, ultrasensitive, flexible tactile sensors based on contact electrification. *Nano Lett.* **14**, 3208–3213 (2014).
3. Yang, W. et al. Triboelectrification based motion sensor for human-machine interfacing. *ACS Appl. Mater.* **6**, 7479–7484 (2014).
4. Chen, J. et al. Personalized keystroke dynamics for self-powered human–machine interfacing. *ACS Nano* **9**, 105–116 (2015).
5. Chen, J. et al. Harmonic-resonator-based triboelectric nanogenerator as a sustainable power source and a self-powered active vibration sensor. *Adv. Mater.* **25**, 6094–6099 (2013).
6. Yang, J. et al. Eardrum-inspired active sensors for self-powered cardiovascular system characterization and throat-attached anti-interference voice recognition. *Adv. Mater.* **27**, 1316–1326 (2015).
7. Zhang, N. et al. A wearable all-solid photovoltaic textile. *Adv. Mater.* **28**, 263–269 (2016).
8. Chen, J. & Wang, Z. L. Reviving vibration energy harvesting and self-powered sensing by a triboelectric nanogenerator. *Joule* **1**, 480–521 (2017).
9. Jun, C. et al. Micro-cable structured textile for simultaneously harvesting solar and mechanical energy. *Nat. Energy* **1**, 16138 (2016).
10. Fan, X. et al. Ultrathin, rollable, paper-based triboelectric nanogenerator for acoustic energy harvesting and self-powered sound recording. *ACS Nano* **9**, 4236–4243 (2015).
11. Lin, Z. et al. Triboelectric nanogenerator enabled body sensor network for self-powered human heart-rate monitoring. *ACS Nano* **11**, 8830–8837 (2017).
12. Wang, Z. L., Chen, J. & Lin, L. Progress in triboelectric nanogenerators as a new energy technology and self-powered sensors. *Energy* **8**, 2250–2282 (2015).
13. Zhang, N., Tao, C., Fan, X. & Chen, J. Progress in triboelectric nanogenerators as self-powered smart sensors. *J. Mater. Res.* **32**, 1628–1646 (2017).
14. Zang, Y. P. et al. Flexible suspended gate organic thin-film transistors for ultra-sensitive pressure detection. *Nat. Commun.* **6**, 6269 (2015).
15. Roh, E., Hwang, B. U., Kim, D., Kim, B. Y. & Lee, N. E. Stretchable, transparent, ultrasensitive, and patchable strain sensor for human−machine interfaces comprising a nanohybrid of carbon nanotubes and conductive elastomers. *ACS Nano* **9**, 6252–6261 (2015).
16. Lee, S. et al. A transparent bending-insensitive pressure sensor. *Nat. Nanotechnol.* **11**, 472–478 (2016).
17. Wu, J. M. et al. Ultrahigh sensitive piezotronic strain sensors based on a ZnSnO3 nanowire/microwire. *ACS Nano* **6**, 4369–4374 (2012).
18. Kaltenbrunner, M. et al. An ultra-lightweight design for imperceptible plastic electronics. *Nature* **499**, 458–463 (2013).
19. Gong, S. et al. A wearable and highly sensitive pressure sensor with ultrathin gold nanowires. *Nat. Commun.* **5**, 3132 (2014).
20. Jansen, K. M. B. Effect of pressure on electrical resistance strain gages. *Exp. Mech.* **37**, 245–249 (1997).
21. Pang, C. et al. A flexible and highly sensitive strain-gauge sensor using reversible interlocking of nanofibres. *Nat. Mater.* **11**, 795–801 (2012).
22. Stassi, S., Cauda, V., Canavese, G. & Pirri, C. F. Flexible tactile sensing based on piezoresistive composites: a review. *Sensors* **14**, 5296–5332 (2014).
23. Cho, S. et al. Large-area cross-aligned silver nanowire electrodes for flexible, transparent, and force-sensitive mechanochromic touch screens. *ACS Nano* **11**, 4346–4357 (2017).
24. Ifa, D. R., Manicke, N. E., Dill, A. L. & Cooks, G. Latent fingerprint chemical imaging by mass spectrometry. *Science* **321**, 805–805 (2008).
25. Kim, H. K., Lee, S. & Yun, K. S. Capacitive tactile sensor array for touch screen application. *Sens. Actuator A-Phys.* **165**, 2–7 (2011).
26. Zardetto, V., Brown, T. M., Reale, A. & Di Carlo, A. Substrates for flexible electronics: a practical investigation on the electrical, film flexibility, optical, temperature, and solvent resistance properties. *J. Polym. Sci. Part B: Polym. Phys.* **49**, 638–648 (2011).
27. Zhao, P., Deng, N., Li, X. W., Ren, C. C. & Wang, Z. Y. Development of highly-sensitive and ultra-thin silicon stress sensor chips for wearable biomedical applications. *Sens. Actuator A-Phys.* **216**, 158–166 (2014).
28. Jiang, F. K., Lee, G. B., Tai, Y. C. & Ho, C. M. A flexible micromachine-based shear-stress sensor array and its application to separation-point detection. *Sens. Actuator A-Phys.* **79**, 194–203 (2000).
29. Burghartz, J. N., Appel, W., Rempp, H. D. & Zimmermann, M. A new fabrication and assembly process for ultrathin Chips. *IEEE Trans. Electron Dev.* **56**, 321–327 (2009).
30. Xu, M. et al. Pressure tunes electrical resistivity by four orders of magnitude in amorphous Ge2Sb2Te5 phase-change memory alloy. *Proc. Natl. Acad. Sci. USA* **109**, E1055–E1062 (2012).
31. Lankhorst, M. H. R., Ketelaars, B. & Wolters, R. A. M. Low-cost and nanoscale non-volatile memory concept for future silicon chips. *Nat. Mater.* **4**, 347–352 (2005).
32. Hosseini, P., Wright, C. D. & Bhaskaran, H. An optoelectronic framework enabled by low-dimensional phase-change films. *Nature* **511**, 206–211 (2014).
33. Nukala, P. et al. Direct observation of metal-insulator transition in single-crystalline germanium telluride nanowire memory devices prior to amorphization. *Nano Lett.* **14**, 2201–2209 (2014).
34. Li, Y., Duerloo, K. A. N., Wauson, K. & Reed, E. J. Structural semiconductor-to-semimetal phase transition in two-dimensional materials induced by electrostatic gating. *Nat. Commun.* **7**, 8 (2016).
35. Waldecker, L. et al. Time-domain separation of optical properties from structural transitions in resonantly bonded materials. *Nat. Mater.* **14**, 991 (2015).
36. Nugaeva, N. et al. Micromechanical cantilever array sensors for selective fungal immobilization and fast growth detection. *Biosens. Bioelectron.* **21**, 849–856 (2005).
37. Pramanik, C., Saha, H. & Gangopadhyay, U. Design optimization of a high performance silicon MEMS piezoresistive pressure sensor for biomedical applications. *J. Micromech. Microeng.* **16**, 2060–2066 (2006).
38. Lang, H. P., Hegner, M. & Gerber, C. Cantilever array sensors. *Mater. Today* **8**, 30–36 (2005).
39. Reed, J., Wilkinson, P., Schmit, J., Klug, W. & Gimzewski, J. K. Observation of nanoscale dynamics in cantilever sensor arrays. *Nanotechnology* **17**, 3873–3879 (2006).
40. Baller, M. K. et al. A cantilever array-based artificial nose. *Ultramicroscopy* **82**, 1–9 (2000).
41. Zhang, W. et al. Density-functional theory guided advances in phase-change materials and memories. *MRS Bull.* **40**, 856–869 (2015).
42. Lee, Y. et al. Wafer-Scale Synthesis and Transfer of Graphene Films. *Nano Lett.* **10**, 490–493 (2010).
43. Dalimier, E. & Salomon, D. Full-field optical coherence tomography: a new technology for 3D high-resolution skin imaging. *Dermatology* **224**, 84–92 (2012).
44. Bai, P. et al. Membrane-based self-powered triboelectric sensors for pressure change detection and its uses in security surveillance and healthcare monitoring. *Adv. Funct. Mater.* **24**, 5807–5813 (2014).